

Original Article

Compressive strengths of Maha Sarakham salt under constant σ_m and constant σ_3 stress paths

Kiattisak Artkhonghan, Suratwadee Sartkaew, Supattra Khamrat,
and Kittitep Fuenkajorn*

*Geomechanics Research Unit, Institute of Engineering,
Suranaree University of Technology, Mueang, Nakhon Ratchasima, 30000 Thailand*

Received: 15 March 2017; Revised: 20 July 2017; Accepted: 4 August 2017

Abstract

True triaxial compression tests were performed to assess the effects of the loading path on the compressive strength and deformability of Maha Sarakham salt. The salt specimens with nominal dimensions of $45 \times 45 \times 90$ mm³ are compressed to failure using a true triaxial load frame. The minimum principal stress was kept constant between 0 and 10 MPa and the mean stress was kept constant between 8 and 85 MPa, while the axial stresses increased at constant rates of 0.1 MPa/s until failure occurred. The results indicated that under constant σ_m stress path the salt fails more easily than under constant σ_3 path. The effects of σ_2 on salt strength can be observed for both constant σ_3 and constant σ_m stress paths. The multi-axial strength criteria that were derived from constant σ_3 strength results may overestimate the stability of the salt around spherical and cylindrical cavities.

Keywords: compression, extension, polyaxial loading, intermediate principal stress

1. Introduction

The effects of intermediate principal stress on rock strengths have long been recognized (Colmenares & Zoback, 2002; Haimson, 2006; Haimson & Chang, 2000; Tiwari & Rao, 2004, 2006; Yang, Zou, & Sui, 2007). It has been found that in a $\sigma_1 - \sigma_2$ diagram, for a given σ_3 , σ_1 at failure initially increases with σ_2 to a certain magnitude, and then it gradually decreases as σ_2 increases further. The effect of σ_2 is larger under higher σ_3 . Cai (2008) offers an explanation of how the intermediate principal stress affects the rock strength based on the results from numerical simulations on fracture initiation and propagation. He states that the intermediate principal stress confines the rock in such a way that fractures can only be initiated and propagated in the direction parallel to σ_1 and σ_2 . The effect of σ_2 is related to the stress-induced anisotropic properties and behaviour of the rock and to the end effect at the interface between the rock surface and the loading platen

in the direction of the σ_2 application. The effect should be smaller in homogeneous and fine-grained rocks than in coarse-grained rocks where pre-existing micro-cracks are not uniformly distributed.

Several failure criteria have been developed to describe the rock strength under true triaxial stress states. Comprehensive reviews of these criteria have been given by Colmenares and Zoback (2002), Haimson (2006), Cai (2008), Yu, Zan, Zhao, and Yoshimine (2002), Al-Ajmi and Zimmerman (2005), Liu, Man, Ma, Zhang, and Gao (2010) and Meyer and Labuz (2013). Among several other criteria, the Mogi and modified Wiebols and Cook criteria are perhaps the most widely used to describe the rock compressive strengths under true triaxial stresses.

It has been recognized that rock strengths obtained from the conventional loading path with constant confining pressure (σ_3) may not truly represent the rock's strengths and deformation around underground openings where the mean stress (σ_m) remains constant and two or three principal stresses change after the opening has been excavated (Mellegard, DeVries, & Callahan, 2005; Mellegard & Pfeifle, 1999; Wawersik & Hannum, 1979). The effects of intermediate principal stress on such stress paths have rarely been

*Corresponding author
Email address: kittitep@sut.ac.th

addressed or quantitatively determined. The representativeness of the multiaxial strength criteria mentioned above has never been experimentally investigated and verified under the loading path of constant mean stress.

The objective of this study is to experimentally determine the effects of stress paths on the compressive strengths of the Maha Sarakham salt. The effects of the two stress paths were assessed under three test (loading) conditions: triaxial compression, polyaxial compression, and triaxial extension. The modes of failure were investigated. The modified Wiebols and Cook, Mogi and Paul-Mohr-Coulomb criteria derived from constant σ_3 test data were used to predict the constant σ_m strength data. The predictive capability of these criteria was assessed. The suitability of these strength criteria for the stability analysis of storage caverns in salt is demonstrated and discussed.

2. Sample Preparation

The specimens were prepared from 63 mm diameter salt cores drilled from depths ranging from 150 m to 250 m. The salt cores belonged to the Middle Salt member of the Maha Sarakham formation. This salt member hosts several solution-mined caverns. The formation is also being considered as a host rock for compressed-air energy storage caverns by the Thai Department of Energy, and for chemical waste disposal by the Office of Atomic Energy for Peace. Warren (1999) gives the origin and geological description of the Maha Sarakham salt.

The salt specimens were virtually pure halite, with a slight amount of clay inclusions (less than 1%). The drilled cores were dry-cut to obtain rectangular specimens with nominal dimensions of 45×45×90 mm³. Over 60 specimens were prepared. No bedding plane was observed in the specimens. Their average density was 2.16±0.09 g/cm³.

Sriapai, Walsri, and Fuenkajorn (2013) determined the mechanical properties of the same salt and reported that the internal friction angle of the salt was 50° and the cohesion was 5.0 MPa. The elastic modulus and Poisson's ratio average were 21.5±2.6 GPa and 0.40±0.04, respectively.

3. Apparatus and Test Method

A true triaxial load frame (Thaweeboon, Dasri, Sartkeaw, & Fuenkajorn, 2016) was used to apply axial stress (σ_1) and lateral stresses (σ_2 and σ_3) to the specimen. The frame was comprised of four main components: three mutually perpendicular load frames; six 100-ton hydraulic cylinders; measurement system; and three hydraulic pumps. The measurement system included pressure transducers, displacement transducers, switching box, and data logger. Neoprene sheets are placed at all interfaces between the loading platens and specimen surfaces to minimize the friction.

The tests are performed under two stress paths: constant confining stress (σ_3 from 0 to 28 MPa) and constant mean stress (σ_m from 8 to 85 MPa). Three test conditions were applied for each stress path: triaxial compression ($\sigma_1 > \sigma_2 = \sigma_3$); polyaxial compression ($\sigma_1 > \sigma_2 > \sigma_3$); and triaxial extension ($\sigma_1 = \sigma_2 > \sigma_3$). Table 1 summarizes the test plan showing the three test conditions with the Lode parameter (Riley, Hobson, & Bence, 1998): $\mu = 1$ for compression; $-1 < \mu < 1$ for polyaxial; and $\mu = -1$ for extension loading, where $\mu = (2\sigma_2 - \sigma_3 - \sigma_1) / (\sigma_3 - \sigma_1)$. All stresses were increased or decreased monotonically under constant rates until failure occurred (drop of σ_1). It is recognized that infinite stress paths can be taken to obtain constant σ_3 and constant σ_m conditions. Monotonic loading conditions under constant rates were used mainly to simplify and limit the number of test variables.

Table 1. Test plan.

		Test conditions		
Stresspath	Compression ($\sigma_1 > \sigma_2 = \sigma_3$) $\mu = 1$	Polyaxial ($\sigma_1 > \sigma_2 > \sigma_3$) $-1 < \mu < 1$	Extension ($\sigma_1 = \sigma_2 > \sigma_3$) $\mu = -1$	
Constant σ_3	<p>Time $\sigma_3 = 1 - 28 \text{ MPa}$</p>	<p>Time $\sigma_3 = 0 - 10 \text{ MPa}$</p>	<p>Time $\sigma_3 = 0 - 10 \text{ MPa}$</p>	
	<p>Time $\sigma_m = 8 - 70 \text{ MPa}$</p>	<p>Time $\sigma_m = 20 - 80 \text{ MPa}$</p>	<p>Time $\sigma_m = 21 - 85 \text{ MPa}$</p>	

After installing the salt specimen into the load frame, the vertical and lateral stresses were simultaneously increased to the predefined σ_3 (for constant σ_3 testing) or σ_m (for constant σ_m testing). This uniform stress was maintained for a minimum of one hour, primarily to ensure that the salt specimen was under an isostatic condition.

For the constant σ_3 path the triaxial compression test was started by increasing σ_1 at the rate of 0.1 MPa/s while σ_2 and σ_3 were equal and maintained constant (between 1 and 28 MPa) until failure occurred. The polyaxial compression tests were performed by increasing σ_1 and σ_2 at different rates while σ_3 was maintained constant between 0 and 10 MPa. For the triaxial extension testing, σ_1 and σ_2 were simultaneously increased at the rate of 0.1 MPa/s while σ_3 was kept constant between 0 and 10 MPa until failure.

Under constant σ_m path, the triaxial compression tests were performed by increasing σ_1 at the rate of 0.1 MPa/s while σ_2 and σ_3 were decreased at the rate of 0.05 MPa/s. Polyaxial compression testing was performed under σ_m that ranged 20-80 MPa. The increase of σ_1 and the decrease of σ_3 were under the same rate of 0.1 MPa/s while σ_2 was kept constant. The triaxial extension tests were performed under σ_m that ranged 21-85 MPa. The increases of σ_1 and σ_2 were made

under the same rate of 0.1 MPa/s while decreasing σ_3 at the rate of 0.05 MPa/s. Photographs were taken of the post-test specimens. The modes of failure were identified.

4. Test Results

The stress-strain curves for both stress paths are given in Figure 1. Both stress paths show that the triaxial compression loading provided a higher strength than the polyaxial compression and triaxial extension loadings. The lowest strengths were obtained from the specimens when they failed under triaxial extension. This agrees with the results obtained by Sriapai, Walsri, and Fuenkajorn (2013) who performed true triaxial testing under constant σ_3 on the same rock salt. Table 2 gives the principal stresses at failure for all stress paths and loading conditions. Table 2 also gives the dilation strength ($\sigma_{1,d}$) for each specimen which is defined as the yield point where the specimen volume starts increasing. Post-test observations suggest that compressive shear failures were predominant in the specimens tested under triaxial compression, while splitting extensile fractures parallel to σ_1 and σ_2 directions dominated under triaxial extension (Table 3). This is true for both stress paths.

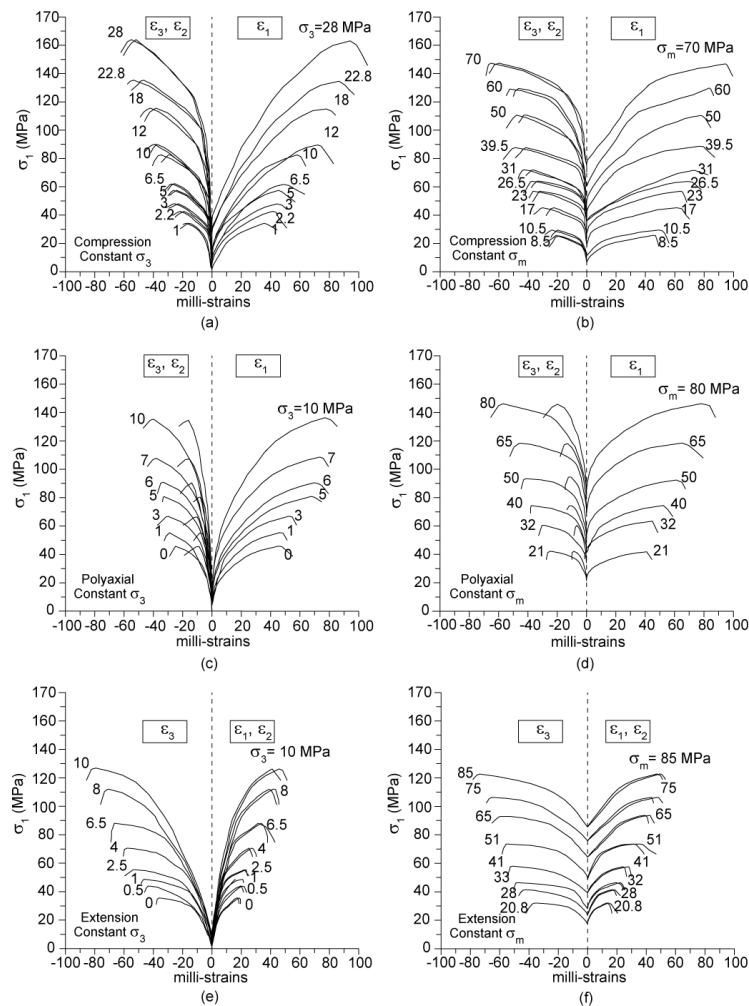


Figure 1. Stress-strain curves for triaxial compression (a, b), polyaxial compression (c, d) and triaxial extension (e, f).

Table 2. Principal stresses at failure and dilation.

Test conditions	Constant σ_3				Constant σ_m			
	$\sigma_{1,d}$ (MPa)	σ_1 (MPa)	σ_2 (MPa)	σ_3 (MPa)	$\sigma_{1,d}$ (MPa)	σ_1 (MPa)	σ_2 (MPa)	σ_3 (MPa)
Compression	20.4	32.2	1.0	1.0	14.4	24.9	0.25	0.25
	24.5	41.9	2.2	2.2	18.1	29.4	1.1	1.1
	28.8	47.1	3.0	3.0	26.8	44.4	3.3	3.3
	35.3	55.8	5.0	5.0	34.5	56.0	6.5	6.5
	39.2	61.9	6.5	6.5	38.2	64.2	7.6	7.6
	55.1	82.3	10.0	10.0	44.4	71.4	10.8	10.8
	56.4	89.1	12.0	12.0	53.1	88.1	15.2	15.2
	73.1	115.0	18.0	18.0	69.3	110.8	19.5	19.5
	82.3	134.6	22.8	22.8	78.2	129.7	25.2	25.2
110.6	163.5	28.0	28.0	83.1	148.5	30.4	30.4	
Polyaxial	25.2	43.0	25.0	0.0	21.8	41.1	21.0	0.9
	33.1	55.5	25.0	1.0	33.8	60.0	32.0	4.0
	41.4	65.3	25.0	3.0	45.6	75.2	40.0	4.8
	54.5	79.8	60.0	5.0	55.9	93.5	50.0	7.0
	59.3	90.5	25.0	6.0	64.9	118.8	65.0	11.2
	64.9	108.7	35.0	7.0	81.0	144.9	80.0	15.1
	88.7	135.3	47.0	10.0				
Extension	25.1	35.0	35.0	0.0	19.0	31.0	31.0	0.5
	26.6	42.1	42.1	0.5	24.4	41.3	41.3	2.3
	32.1	49.0	49.0	1.0	25.6	47.6	47.6	3.5
	34.8	55.2	55.2	2.5	36.2	58.9	58.9	5.5
	41.3	69.9	69.9	4.0	41.6	73.5	73.5	6.5
	58.4	89.1	89.1	6.5	51.6	92.4	92.4	9.8
	72.2	112.0	112.0	8.0	64.9	106.7	106.7	11.9
	85.5	127.0	127.0	10.0	72.2	121.1	121.1	12.9

Table 3. Cohesion and friction angle calculated based on Coulomb criterion.

Stress paths	Test conditions	ϕ (Degrees)	c (MPa)
Constant σ_3	Compression	43	3.9
	Extension	52	5.5
	Polyaxial	54	6.8
Constant σ_m	Compression	39	3.2
	Extension	48	4.8
	Polyaxial	50	6.3

5. Shear-normal Stress Diagrams

Based on the Coulomb criterion, the cohesion (c) and internal friction angle (ϕ) of the salt were calculated. This was done primarily to reveal the effects of stress path and stress condition on the widely used Coulomb criterion and its parameters (c and ϕ). The principal stresses at failure ($\sigma_{1,f}$, $\sigma_{3,f}$) can be written as a function of the uniaxial compressive strength (σ_c) as:

$$\sigma_{1,f} = \sigma_c + \sigma_{3,f} \tan^2\alpha \tag{1}$$

$$\sigma_c = 2c \tan \alpha \tag{2}$$

$$\alpha = (\pi/4) + 1/2\phi \tag{3}$$

Regression analysis of the above equations and the test data was performed to determine the cohesion and friction angle (Figure 2 and Table 4). It was found that if only 2-dimensional stresses at failure were considered, the salt specimens under constant σ_m path showed relatively lower strengths than those under constant σ_3 path. This held true for all stress conditions. For both stress paths the triaxial compression gives lower shear strength than those of the polyaxial compression and triaxial extension. This may be because the specimens subjected to the triaxial compression could dilate more easily (in the σ_3 -direction) than those of the other two test conditions. As a result shear fractures can be induced more easily in the specimens compared to the other two stress conditions.

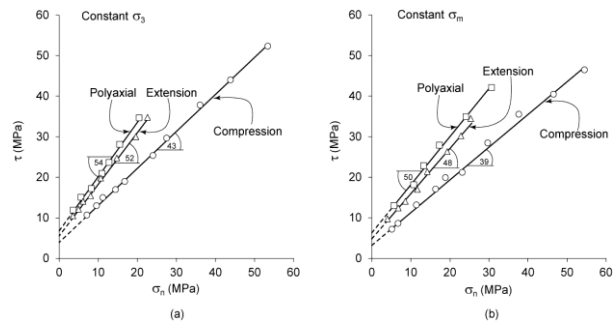
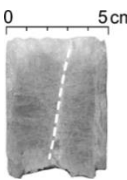
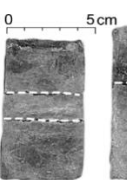
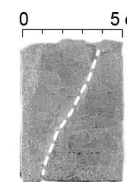
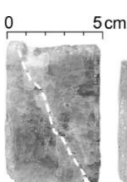
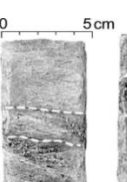


Figure 2. Shear strengths-normal stresses relation based on the Coulomb criterion.

Table 4. Some post-test specimens.

Stress paths	Test conditions					
	Compression ($\sigma_1 > \sigma_2 = \sigma_3$) $\mu = 1$		Polyaxial ($\sigma_1 > \sigma_2 > \sigma_3$) $-1 < \mu < 1$		Extension ($\sigma_1 = \sigma_2 > \sigma_3$) $\mu = -1$	
Constant σ_3						
	$\sigma_3 = 23 \text{ MPa}$	28 MPa	5 MPa	7 MPa	8 MPa	1 MPa
Constant σ_m						
	$\sigma_m = 23 \text{ MPa}$	28 MPa	23 MPa	28 MPa	23 MPa	28 MPa

6. Strength Criteria

To demonstrate the effect of the stress paths the modified Wiebols and Cook, Mogi and Paul-Mohr-Coulomb strength criteria derived from the constant σ_3 test data were used to predict the salt strengths under constant σ_m test data. There criteria have been widely used and have claimed that they can adequately predict the rock strengths under multi-axial stress states (Colmenares & Zoback, 2002; Meyer & Labuz, 2013; Sriapai, Walsri, & Fuenkajorn, 2013). The predictive capability of the three criteria was determined and compared using the mean misfit as an indicator. The lower misfit value indicated the better predictability of the criterion. The mean misfit (\bar{s}) for each criterion can be calculated by (Riley, Hobson, & Bence, 1998)

$$\bar{s} = \frac{1}{m} \sum_i^m s_i \tag{4}$$

where

$$s_i = \sqrt{\frac{1}{n} \sum_j^n (\sigma_{1,j}^{calc} - \sigma_{1,j}^{test})^2}$$

$\sigma_{1,j}^{calc}$ = predicted strengths

$\sigma_{1,j}^{test}$ = measured strengths

n = number of the intermediate principal stresses used for each σ_3 level

m = number of σ_3 levels

6.1 Modified Wiebols and Cook criterion

The modified Wiebols and Cook criterion proposed by Zhou (1994) was originally developed by Wiebols and Cook (1968) based on the additional energy stored around Griffith cracks due to the sliding of crack surfaces over each other. The modified version defines $J_2^{1/2}$ at failure in terms of σ_m as:

$$J_2^{1/2} = A + B\sigma_m + C\sigma_m^2 \tag{5}$$

The constants A, B, and C depend on friction angle, cohesion, and uniaxial compressive strength. Table 4 summarizes the parameters A, B, and C for the calculation. For both stress paths they can be determined under the conditions where $\sigma_2 = \sigma_3$ (triaxial compression), as follows (Wiebols & Cook, 1968):

$$C = \frac{\sqrt{27}}{2C_1 + (q-1)\sigma_3 - \sigma_c} \times \left(\frac{C_1 + (q-1)\sigma_3 - \sigma_c}{2C_1 + (2q+1)\sigma_3 - \sigma_c} - \frac{q-1}{q+2} \right) \tag{6}$$

where

$$C_1 = (1 + 0.6\mu_i)\sigma_c$$

σ_c = uniaxial compressive strength of the rock

$$\mu_i = \tan\phi$$

$$q = \{(\mu_i^2 + 1)^{1/2} + \mu_i\}^2 = \tan^2(\pi/4 + \phi/2)$$

$$B = \frac{\sqrt{3}(q-1)}{q+2} - \frac{C}{3}(2\sigma_c + (q+2)\sigma_3) \tag{7}$$

$$A = \frac{\sigma_c}{\sqrt{3}} - \frac{\sigma_c}{3} B - \frac{\sigma_c^2}{9} C \quad (8)$$

$$\bar{B} = \frac{\sin \varphi_c - \sin \varphi_e}{2V_o \sin \varphi_c \sin \varphi_e} \quad (14)$$

The criterion can also be expressed in terms of the principal stresses at failure as:

$$\sigma_1 = \left[\frac{6(\psi - \chi) - 3(A + B\sigma_m)}{C\sigma_m} \right] (\sigma_2 + \sigma_3) \quad (9)$$

$$\bar{C} = -\frac{1 + \sin \varphi_e}{2V_o \sin \varphi_e} \quad (15)$$

where $\psi = (\sigma_1^2 + \sigma_2^2 + \sigma_3^2)$

$$\chi = (\sigma_1\sigma_2 + \sigma_1\sigma_3 + \sigma_2\sigma_3)$$

Figure 3a compares constant σ_m test data with the predictions from the modified Wiebols and Cook criterion derived from constant σ_3 test data in the form of $\sigma_1 - \sigma_2$ diagrams. The calculations were made for $\sigma_3 = 0, 1, 3, 5, 7,$ and 10 MPa. The parameters of the modified Wiebols and Cook predictions were derived for each stress path. It was found that the criterion derived from constant σ_3 data could not adequately describe the salt strength obtained under constant σ_m stress path ($\bar{S}=10.5$, Figure 3a). They tend to overestimate the strength results.

where V_o is the (theoretical) uniform triaxial tensile strength, and φ_c and φ_e are internal friction angles for triaxial compression and extension stress states. Table 5 gives the numerical values of these constants. The calibration uses the test data obtained under constant σ_3 stress path given in Table 2.

Figure 3c compares the constant σ_m test data with the Paul-Mohr-Coulomb criterion predictions calibrated from the constant σ_3 test data. The calculations were made for $\sigma_3 = 0, 1, 3, 5, 7,$ and 10 MPa. The criterion could not describe the effect of σ_2 . Its prediction exhibited a series of strength lines from $\sigma_2=\sigma_3$ ($\mu=1$) to $\sigma_1=\sigma_2$ ($\mu=-1$) test conditions. Even though the criterion could describe the salt strengths under triaxial compression ($\sigma_2=\sigma_3$), it underestimated the polyaxial strengths ($\sigma_1 \neq \sigma_2 \neq \sigma_3$) and overestimated the triaxial extension strengths ($\sigma_1 = \sigma_2$).

6.2 Mogi criterion

The Mogi criterion defines τ_{oct} in terms of the effective mean stress ($\sigma_{m,2}$) using a power relation (You, 2009):

$$\tau_{oct} = A' \sigma_{m,2}^{B'} \quad (10)$$

$$\sigma_{m,2} = (\sigma_1 + \sigma_3) / 2 \quad (11)$$

7. Potential Applications

The three strength criteria studied above were applied to determine the factors of safety of the salt around cylindrical and spherical cavities in an infinite salt mass subjected to uniform external pressure (P_o). No internal pressure was applied. This was primarily to demonstrate what would occur when the strength criteria that are derived from the constant σ_3 and constant σ_m test data were used to predict the stability condition of the salt around the cavities. For this demonstration P_o ranged from 5 to 20 MPa.

where A' and B' are empirical parameters depending on the materials. Figure 3b compares the constant σ_m test results with the Mogi criterion derived from constant σ_3 test data. The predictions notably overestimate the strengths of the salt, particularly under high σ_3 values.

6.3 Paul-Mohr-Coulomb criterion

The Paul-Mohr-Coulomb criterion was originally developed by Paul (1968). It is a linear function of three principal stresses. The modified version by Meyer and Labuz (2013) defines $\sigma_1, \sigma_2,$ and σ_3 at failure in terms of three identifiable material constants ($\bar{A}, \bar{B},$ and \bar{C}) as:

$$1 = \bar{A} \sigma_1 + \bar{B} \sigma_2 + \bar{C} \sigma_3 \quad (12)$$

The material constants $\bar{A}, \bar{B},$ and \bar{C} can be determined under the test conditions where $\sigma_2=\sigma_3$ (triaxial compression) and $\sigma_1=\sigma_2$ (triaxial extension) as follows (Meyer & Labuz, 2013):

$$\bar{A} = \frac{1 - \sin \varphi_c}{2V_o \sin \varphi_c} \quad (13)$$

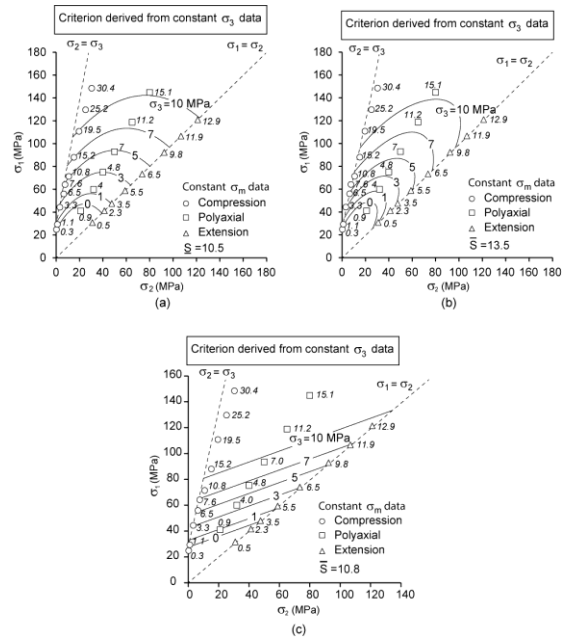


Figure 3. Salt strengths under constant σ_m path compared with the modified Wiebols and Cook (a), Mogi (b), and Paul-Mohr-Coulomb (c) predictions derived from constant σ_3 path.

Table 5. Parameters for strength criteria calibrated from constant σ_3 and constant σ_m stress paths.

Criteria	Calibrated Parameters	
	Constant σ_3	Constant σ_m
Modified Wiebols and Cook	$c = 3.9$ MPa	$c = 3.2$ MPa
	$\phi = 43^\circ$	$\phi = 39^\circ$
	$\sigma_c = 18.0$ MPa	$\sigma_c = 15.4$ MPa
	$\sigma_3 = 0,$	$\sigma_3 = 0,$
	$A = 3.597$ MPa,	$A = 3.406$ MPa,
	$B = 1.272,$	$B = 1.167,$
	$C = -0.023$ MPa ⁻¹	$C = -0.024$ MPa ⁻¹
	$\sigma_3 = 1,$	$\sigma_3 = 1,$
	$A = 3.384$ MPa,	$A = 3.133$ MPa,
	$B = 1.296,$	$B = 1.174,$
	$C = -0.021$ MPa ⁻¹	$C = -0.022$ MPa ⁻¹
	$\sigma_3 = 3,$	$\sigma_3 = 3,$
	$A = 3.053$ MPa,	$A = 2.833$ MPa,
$B = 1.332,$	$B = 1.268,$	
$C = -0.018$ MPa ⁻¹	$C = -0.020$ MPa ⁻¹	
$\sigma_3 = 5,$	$\sigma_3 = 5,$	
$A = 2.809$ MPa,	$A = 2.601$ MPa,	
$B = 1.359,$	$B = 1.310,$	
$C = -0.015$ MPa ⁻¹	$C = -0.018$ MPa ⁻¹	
$\sigma_3 = 7,$	$\sigma_3 = 7,$	
$A = 2.622$ MPa,	$A = 2.445$ MPa,	
$B = 1.379,$	$B = 1.355,$	
$C = -0.014$ MPa ⁻¹	$C = -0.016$ MPa ⁻¹	
$\sigma_3 = 10,$	$\sigma_3 = 10,$	
$A = 2.312$ MPa,	$A = 2.154$ MPa,	
$B = 1.422, C = -$	$B = 1.398, C = -$	
0.012 MPa ⁻¹	0.014 MPa ⁻¹	
Mogi	$A' = 1.4$	$A' = 1.32$
	$B' = 0.84$	$B' = 0.81$
Paul-Mohr-Coulomb	$V_o = 6.5$ MPa	$V_o = 6.5$ MPa
	$\phi_c = 43^\circ$	$\phi_c = 39^\circ$
	$\phi_e = 52^\circ$	$\phi_e = 48^\circ$
	$\bar{A} = 0.036$ MPa ⁻¹	$\bar{A} = 0.044$ MPa ⁻¹
	$\bar{B} = -0.015$ MPa ⁻¹	$\bar{B} = -0.019$ MPa ⁻¹
	$\bar{C} = -0.174$ MPa ⁻¹	$\bar{C} = -0.180$ MPa ⁻¹

For a cylindrical cavity in the vertical position, the stress distributions can be calculated using the Kirsch solution (Brady & Brown, 1985). The radial (σ_r) and tangential (σ_θ) stresses can be written as:

$$\sigma_r = (1 - \frac{a^2}{r^2})P_o \tag{16}$$

$$\sigma_\theta = (1 + \frac{a^2}{r^2})P_o \tag{17}$$

where a =cavity radius and r =radial distance from the center. Under plane strain condition the axial stress (σ_z) can be determined by: $\sigma_z = [v/(1-v)] (\sigma_r + \sigma_\theta)$. For a simplified analysis here, v is assumed to be 0.5. The surrounding salt was subjected to polyaxial compression, where the radial stress is the lowest, which represented σ_3 . The axial stress was σ_2 , and the tangential stress was the greatest which represented σ_1 .

At $r=a$ equations (16) and (17) become

$$\sigma_r = 0 \tag{18}$$

$$\sigma_\theta = 2P_o \tag{19}$$

$$\sigma_z = P_o \tag{20}$$

At this point the induced octahedral shear stress ($\tau_{oct,i}$), the second order deviatoric stress invariants ($J_{2,i}$), and the major principal stress ($\sigma_{1,i}$) can be calculated as:

$$\tau_{oct,i} = \frac{\sqrt{6}}{3} P_o \tag{21}$$

$$J_{2,i}^{1/2} = \frac{\sqrt{3}}{\sqrt{2}} \frac{\sqrt{6}}{3} P_o \tag{22}$$

$$\sigma_{1,i} = 2P_o \tag{23}$$

For a spherical cavity the radial and tangential stresses can be calculated using the solutions given by Brady & Brown (1985). Under uniform external pressure P_o the two tangential stresses are equal. The radial and tangential stresses for this case are as follows:

$$\sigma_r = (1 - \frac{a^3}{r^3})P_o \tag{24}$$

$$\sigma_\theta = (1 + \frac{a^3}{2r^3})P_o \tag{25}$$

where σ_r is the radial stress and σ_θ represents the two tangential stresses. Salt around a spherical cavity is subjected to triaxial extension conditions. The two tangential stresses represent major principal stresses, and the radial stress represents minor principal stress.

At $r=a$ equations (24) and (25) become

$$\sigma_r = 0 \tag{26}$$

$$\sigma_\theta = \frac{3}{2} P_o \tag{27}$$

At $r=a$ the induced octahedral shear stress ($\tau_{oct,i}$), the second order deviatoric stress invariants ($J_{2,i}$), and the major principal stress ($\sigma_{1,i}$) for the spherical cavity can be calculated as:

$$\tau_{oct,i} = \frac{1}{\sqrt{2}} P_o \tag{28}$$

$$J_{2,i}^{1/2} = \frac{\sqrt{3}}{2} P_o \tag{29}$$

$$\sigma_{1,i} = \frac{3}{2} P_o \tag{30}$$

The stress distributions for the cylindrical and spherical cavities above represent the final stress states after the cavities have been developed. It is assumed that these stresses are monotonically changed from the hydrostatic stress P_o to the final stress states as defined in equations (16), (17), (23), and (24). For example, for the spherical cavity, at $r=a$, the two tangential stresses increase from P_o to σ_θ , and the

radial stress reduces from P_o to 0. The stress paths at which these stresses reach their final values are different from those under conventional laboratory testing where the salt is under constant σ_3 until failure. Since the effect of the stress path studied was revealed under failure conditions, a strength criterion is needed to compare its prediction with the stress distributions induced around the cavities.

To show the effects of stress path on the stability determination, the three criteria calibrated in Section 6 were used to determine the stability condition at the boundary of the spherical and cylindrical cavities. The factor of safety (FS) calculations can be made as follows:

$$\text{Modified Wiebols and Cook: } FS = J_2^{1/2} / J_{2,i}^{1/2} \quad (31)$$

$$\text{Mogi: } FS = \tau_{oct} / \tau_{oct,i} \quad (32)$$

$$\text{Paul-Mohr-Coulomb: } FS = \sigma_1 / \sigma_{1,i} \quad (33)$$

where $J_2^{1/2} = (A + BP_o + CP_o^2)$, $\tau_{oct} = A'[(\sigma_\theta) / 2]^{B'}$, $\sigma_1 = [1 - (\bar{B} \sigma_2)] / \bar{A}$ and $\sigma_2 = P_o$ (for cylindrical cavity), $= 3P_o/2$ (for spherical cavity).

The parameters of each criterion are derived from the test data under both constant σ_3 and constant σ_m stress paths (Table 5). Figure 4 plots the factors of safety (FS) as a function of P_o from 5 to 20 MPa. It is clear from the diagrams in Figure 4 that any strength criterion derived from the constant σ_3 test data always overestimates the stability condition of the surrounding salt. This demonstration suggests that the FS calculation from the constant σ_m test data is more preferable than from the constant σ_3 test data. All three criteria show decreases of FS as P_o increases (or depth increases).

The Mogi criterion that over predicts the strength data (Figure 3b) shows lower FS values than the other two criteria. This is probably because the strength predictions from Mogi criterion (Figure 3) were lower than those of the Modified Wiebols and Cook and Paul-Mohr-Coulomb criteria. The discrepancies of the factors of safety obtained among the three multi-axial strength criteria were mainly due to the fact that they were formulated by different mathematical forms. Quadratic (nonlinear) equations use the Modified Wiebols and Cook criterion while the Paul-Mohr-Coulomb criterion uses a set of linear equations. The Mogi criterion uses the shear strength in three-dimensional form (τ_{oct}) but considers only two-dimensional stress for the mean value ($\sigma_{m,2}$). For both cavity shapes the FS values from all criteria calculated from constant σ_3 strength data were always greater than those obtained from the constant σ_m data. This implied that the criteria derived from constant σ_3 strength results may overestimate the stability of salt around storage caverns.

8. Discussion and Conclusions

It is clear from the test results that under constant σ_m stress path the salt fails at a lower value of σ_1 than under constant σ_3 path. This observation agrees well with those obtained by Mellegard and Pfeifle (1999) on rock salt. This could be explained by the fact that when σ_2 or σ_3 or both decrease as σ_1 increases, the salt can dilate along the σ_2 or σ_3 or both directions more easily than when it is subject to

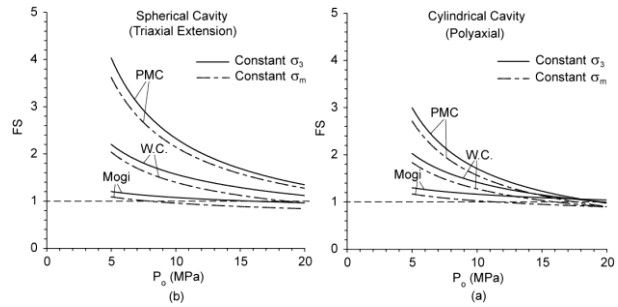


Figure 4. Factors of safety at boundary of cylindrical cavity (a) and spherical cavity (b) as a function of P_o .

constant confinement while σ_1 is increased. The constant σ_m stress path is likely to be the same under the conditions imposed on the rock salt after an opening is excavated.

The effects of σ_2 on salt strength can be observed for both constant σ_3 and constant σ_m stress paths (Figure 3). The increase of σ_2 or decrease of μ resulted in a reduction of the salt strength, which agrees with the experimental results obtained by Mellegard, DeVries, and Callahan (2005) Sriapai, Walsri, and Fuenkajorn (2013) and Hunsche (1991). This is true for both constant σ_3 and constant σ_m paths. A possible explanation is that when the salt is subjected to high principal stresses in two directions, it tends to dilate along the third direction and eventually induces extension failure with the fracture planes parallel to the high stress directions.

It was found that the three multi-axial criteria derived from (conventionally used) constant σ_3 stress paths could not adequately describe the strengths of rock salt subjected to the constant σ_m stress paths. All criteria overestimated the constant σ_m strength results. Even though the Paul-Mohr-Coulomb criterion could well describe the triaxial compressive strengths ($\sigma_2 = \sigma_3$), it greatly overestimates the salt strength under triaxial extension test conditions, and underestimates the strengths for the polyaxial stress state (Figure 3c). This finding suggests that to predict the salt strengths under *in situ* conditions (constant σ_m stress path), the criterion parameters should be calibrated from the constant σ_m test data.

The stress distributions around cylindrical and spherical cavities are polyaxial compression and triaxial extension rather than the triaxial compression as typically simulated by the conventional test method. As a result the strength criteria developed from constant σ_m stress path with various σ_2 magnitudes provides results closer to the actual *in situ* stress conditions.

Under the same P_o , the FS values from the Paul-Mohr-Coulomb criterion for the spherical cavities were greater than those from the cylindrical cavities because the calibrated strength envelope over predicted the triaxial extension test data and under predicted the polyaxial strength data. The Mogi criterion gave lower FS values for the spherical cavity than for the cylindrical cavity. This is probably because the criterion under predicted the triaxial extension strengths while it over predicted the polyaxial strength results.

The specimen size used in this study was relatively small. Recognizing the size effects on the rock strengths, larger specimens are preferable. The strengths obtained under

all test schemes possibly overestimated the salt strengths under *in situ* condition due to the scale effect. Nevertheless, the issue of the size effect would not change the main conclusions drawn that the salt strengths increase with the Lode parameter and that salt compressed under constant σ_3 path yields greater compressive strengths than those under constant σ_m path.

Acknowledgements

This study was funded by Suranaree University of Technology and by the Higher Education Promotion and National Research University of Thailand. Permission to publish this paper is gratefully acknowledged.

References

- Al-Ajmi, A. M., & Zimmerman, R. W. (2005). Relation between the Mogi and the Coulomb failure criteria. *International Journal of Rock Mechanics and Mining Sciences*, 42, 431-439. doi:10.1016/j.ijrmms.2004.11.004
- Brady, B. H. G., & Brown, E. T. (1985). *Rock mechanics for underground mining*. New York, NY: Springer.
- Cai, M. (2008). Influence of stress path on tunnel excavation response-numerical tool selection and modeling strategy. *Tunnelling and Underground Space Technology*, 23, 618-628. doi: 10.1016/j.tust.2007.11.005
- Colmenares, L., & Zoback, M. D. (2002). A statistical evaluation of intact rock failure criteria constrained by polyaxial test data for five different rocks. *International Journal of Rock Mechanics and Mining Sciences*, 39, 695-729. doi:10.1016/S1365-1609(02)00048-5
- Haimson, B. (2006). True triaxial stresses and the brittle fracture of rock. *Pure and Applied Geophysics*, 163, 1101-1113. doi: 10.1007/S00024-006-0065-7
- Haimson, B., & Chang, C. (2000). A new true triaxial cell for testing mechanical properties of rock, and its use to determine rock strength and deformability of Westerly granite. *International Journal of Rock Mechanics and Mining Sciences*, 37(1), 285-296. doi: 10.1016/S1365-1609(99)00106-9
- Hunsche, U. (1991). True triaxial failure test on cubic rock salt samples experimental methods and results. *Proceedings of the IUTAM-Symposium*, 525-536. doi:10.1007/978-3-642-84833-9_47
- Liu, X. Y., Man, L. J., Ma, S. N., Zhang, X. W., & Gao, L. (2010). Comparative study of four failure criteria for intact bedded rock salt. *International Journal of Rock Mechanics and Mining Sciences*, 48, 341-346.
- Mellegard, K. D., & Pfeifle, T. W. (1999). Laboratory evaluation of mechanical properties of rock using an automated triaxial compression test with a constant mean stress criterion. *American Society for Testing and Materials*. doi: 10.1520/STP13320S
- Mellegard, K. D., DeVries, K. L., & Callahan, G. D. (2005). Lode angle effects on the deformational properties of natural rock salt. *Proceeding of the 40th US Rock Mechanics Symposium*, 949-962.
- Meyer, J. P., & Labuz, J. F. (2013). Linear failure criteria with three principal stresses. *International Journal of Rock Mechanics and Mining Sciences*, 60, 180-187. doi:10.1016/j.ijrmms.2012.12.040
- Paul, B. (1968). Generalized pyramidal fracture and yield criteria. *International Journal of Solids and Structures*, 4, 175-96. doi: 10.1016/0020-7683(68)90010-3
- Poulos, H. G., & Davis, E. H. (1974). *Elastic solutions for soil and rock mechanics*. New York, NY: Wiley.
- Riley, K. F., Hobson, M. P., & Bence, S. J. (1998). *Mathematical methods for physics and engineering*. Cambridge, England: Cambridge University Press.
- Sriapai, T., Walsri, C., & Fuenkajorn, K. (2013). True-triaxial compressive strength of MahaSarakhm salt. *International Journal of Rock Mechanics and Mining Sciences*, 61, 256-265. doi: 10.1016/j.ijrmms.2013.03.010
- Thaweeboon, S., Dasri, R., Sartkaew, S., & Fuenkajorn, K. (2016). Strength and deformability of small-scale rock mass models under large confinements. *Bulletin of Engineering Geology and the Environment*, 1-13. doi:10.1007/s10064-016-0871-9
- Tiwari, R. P., & Rao, K. S. (2004). Physical modeling of a rock mass under a true triaxial stress state. *International Journal of Rock Mechanics and Mining Sciences*, 41(Suppl.1), 396-401. doi:10.1016/j.ijrmms.2003.12.073
- Tiwari, R. P., & Rao, K. S. (2006). Post failure behavior of a rock mass under the influence of triaxial and true triaxial confinement. *Engineering Geology*, 84, 112-129. doi:10.1016/j.enggeo.2006.01.001
- Warren, J. K. (1999). *Evaporites: Their evolution and economics*. Oxford, England: Blackwell Science.
- Wawersik, W. R., & Hannum, D. W. (1979). Mechanical behavior of New Mexico rock salt in triaxial compression up to 200°C. *Journal of Geophysical Research*, 82(B2), 891-900. doi: 10.1029/JB085iB02p00891
- Wiebols, G. A., & Cook, N. G. W. (1968). An energy criterion for the strength of rock in polyaxial compression. *International Journal of Rock Mechanics and Mining Sciences*, 5, 529-549. doi: 10.1016/0148-9062(68)90040-5
- Yang, X. L., Zou, J. F., & Sui, Z. R. (2007). Effect of intermediate principal stress on rock cavity stability. *Journal of Central South University of Technology*, 14(s1), 165-169. doi:10.1007/s11771-007-0237-3
- You, M. (2009). True-triaxial strength criteria for rock. *International Journal of Rock Mechanics and Mining Sciences*, 46, 115-127. doi:10.1016/j.ijrmms.2008.05.008
- Yu, M. H., Zan, Y. W., Zhao, J., & Yoshimine, M. (2002). A unified strength criterion for rock material. *International Journal of Rock Mechanics and Mining Sciences*, 39(8), 975-989. doi: 10.1016/S1365-1609(02)00097-7
- Zhou, S. A. (1994). Program to model the initial shape and extent of borehole breakout. *Computers and Geosciences*, 20(7-8), 1143-60. doi:10.1016/0098-3004(94)90068-X